Geophys. J. R. astr. Soc. (1987) **90**, 285–303

Applications of seismic travel-time tomography

R. Phillip Bording*, Adam Gersztenkorn, Larry R. Lines, John A. Scales and Sven Treitel *Amoco Production Company, Research Center, PO Box 3385, Tulsa, Oklahoma 74102, USA*

Accepted 1986 December 2. Received 1986 November 18; in original form 1986 June 19

Summary. This paper describes the application of tomography to seismic travel-time inversion. There are various implementations of travel-time tomography. In reflection tomography, sources and receivers are on the surface of the Earth and the principal seismic events are reflections from subsurface velocity discontinuities. In transmission tomography, sources and/or receivers may be buried beneath the surface and the events correspond to direct, or unreflected, arrivals; this is the analogue of medical tomography. There are also cases in which both direct as well as reflected arrivals are important, such as in Vertical Seismic Profiling. The latter is a direct application of the first two, but is not discussed in any detail here. It is also shown how the iterative use of travel-time tomography and depth migration can produce much enhanced subsurface images. Examples of both transmission tomography and reflection tomography combined with depth migration illustrate the methods.

Key words: seismic tomography, inverse theory, migration, velocity analysis, travel-time inversion

1 Procedure

The word tomography comes from the Greek 'tomos' meaning section or slice. Thus tomography is based on the idea that an observed data set consists of integrals along lines or rays (i.e. projections) of some physical quantity. The data are observed from outside the domain of this quantity and the purpose of tomography is to reconstruct a model of the quantity such that the model's projected data agree approximately with measurements. A classic geophysical tomography problem is the reconstruction of a velocity model for the Earth, or some portion thereof, from observed travel times. For a general discussion of tomography the reader is referred to the works of Herman (1980), Deans (1983), and Worthington (1984), and the references cited therein.

The focus of this paper will be the geophysical tomography problem for travel times. There are two distinct cases to consider. First, there is the reflection problem (the most

* Now at: Minnesota Supercomputer Center, Inc., PO Box 1486, Claremore, Oklahoma 74018, USA.

common in exploration seismology), in which both source and receiver are at the surface of the Earth. Secondly, there is the transmission problem in which the sources and/or receivers may be in boreholes beneath the surface; or in some cases the source and receiver positions are such that they are joined by refracted raypaths. Hybrid problems, such as VSP, in which both reflection and refraction are important represent a straightforward generalization of these two cases. In any event the essence of travel-time tomography is the fact (to the extent that ray theory is valid) that the travel-time associated with a given ray (i.e. the total transit time from source to receiver) is the integrated slowness along that ray. In the two-dimensional (2-D) case, one has

$$t(\text{ray}) = \int_{\text{ray}} s(x, z)\, dl, \tag{1}$$

where x and z are horizontal and vertical coordinates, dl is the differential distance along the ray, and $s(x, z) = 1/v(x, z)$ is the slowness (reciprocal velocity) at the point (x, z).

A fundamental difficulty with the seismic tomography problem is that the ray path itself depends on the unknown slowness. Therefore (1) is non-linear in the slowness. The approach traditionally used in tomography is to linearize (1) about some initial, or reference, slowness model. In other words, instead of solving (1) for s, one solves some approximation to (1) for the perturbations in s from an initial model. When this is done, the discrete form of the linearized equation for a collection of rays is

$$\Delta t = D\Delta s, \tag{2}$$

where Δt is a vector whose components are the differences between the travel times computed for the model and the observed travel times, Δs is a vector whose components are the differences in slowness between the initial model and the solution, and D is a matrix whose element D_{ij} is the distance the ith ray travels in the jth cell (Fig. 1). As a consequence of Fermat's principle, perturbations in ray path are second order with respect to perturbations in slowness (Spofford & Stokes 1984).

Various discretizations of the model are possible; to simplify the discussion it will be assumed that the model is covered with square cells of constant size, and within each cell the slowness is constant. The generalization to variable-sized cells, which is important for dealing with limited resolution and complex geology, is largely a matter of book-keeping (e.g. Christoffersson & Husebye 1979).

The basic tomography procedure is to first pick travel-times from unstacked seismic sections, or measure them in the field (Gustavsson *et al.* 1986). Rays are then traced through the original model for all of the events for which travel times have been picked. The simplest ray tracing ignores Snell's law at all cell boundaries, so that sources and receivers are joined by straight lines and the distances D_{ij} are computed by simple trigonometry. More realistic ray tracing procedures either bend the rays at each cell boundary according to Snell's law or numerically integrate the ray equations; the distances D_{ij} are again easily computed. In the case of reflection tomography, allowance must be made for a ray to be reflected at geologic interfaces. Strictly speaking, rays could reflect from every cell boundary, but it will be assumed that velocity contrasts at the cell boundaries are small enough so that such reflections can be neglected. Reflections will be allowed to occur only at prescribed interfaces (Cassell 1982; Langan, Lerche & Cutler 1985).

The ith row of the D matrix describes the path of the ith ray from source to receiver (Fig. 1). The number of rows equals the number of rays, whereas the number of columns is equal to the number of cells used to describe the model. In general D will have more rows than columns since one wants the model to be illuminated with as many rays as possible. In other

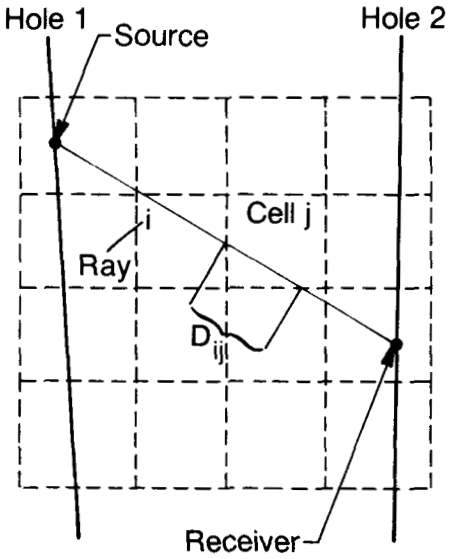

Figure 1. A subsurface region and its discretization into cells. The ith ray travels a distance D_{ij} in the jth cell. (After Dines & Lytle 1979.)

words, if one were to use the same number of cells as rays, the cells would, in parts of the model, be smaller than the resolving power of the data. Accordingly, a generalized solution to (2) is computed. The solution is a set of slowness perturbations Δs which are added to the initial slowness model to produce an updated model. At this stage the procedure can be repeated with the updated slowness model. This requires tracing rays through the updated model if Snell's law is to be satisfied; in the case of straight rays, the distance elements D_{ij} remain fixed and need only be determined once. In either case travel times must be recomputed for the updated slowness model. This iterative process can continue until some previously established stopping criterion has been satisfied. The set of cell velocities obtained in this way is called a tomogram.

Our formulation of reflection tomography distinguishes between the non-reflecting cell boundaries and the explicitly defined subsurface reflecting interfaces (Fig. 2); these

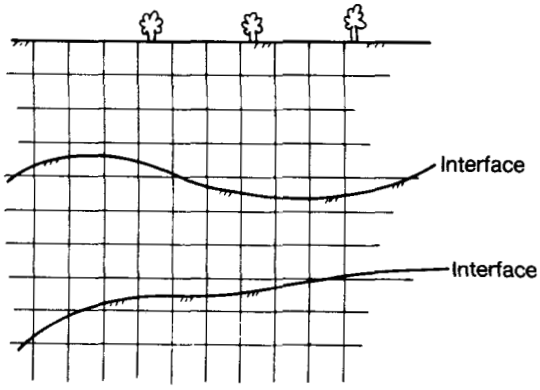

Figure 2. Parameterization of the subsurface in terms of velocity cells and interfaces. In the inversion, the velocities are assumed to be constant within cells.

reflectors can be expressed either analytically or numerically, e.g. as splines. The starting model consists of the initial cell slownesses along with a set of initial reflecting interfaces. Bishop *et al.* (1985) perform least-squares inversion for both cell velocities and interface geometry. Williamson (1984), on the other hand, assumes that the reflecting boundary positions are known and uses tomography only to infer the velocity field. Similar approaches can be found in Tarantola & Nercessian (1984), Nercessian, Hirn & Tarantola (1984), and Neumann (1981).

In this paper an alternative approach is used (Whitmore & Lines 1986; Stork & Clayton 1985) in which each updated slowness model is the input for a depth migration scheme. This could be pre-stack or post-stack migration, since in either case travel-time inversion is used to produce a velocity model and migration is used to position the reflectors. Migration and velocity inversion are obviously not completely independent since migration images jumps in the velocity. The repeated use of the travel-time tomography followed by depth migration will be called 'Iterative Tomographic Migration'. Again, this dual procedure is repeated until a previously established stopping criterion has been satisfied. In the numerical examples it will be seen that a single tomographic velocity inversion followed by migration is adequate; of course, this need not always be so.

We favour Iterative Tomographic Migration because it combines a good feature of tomography, namely velocity inversion, with a good feature of depth migration, namely imaging of the interfaces. In fact, good performance of a depth migration scheme is predicated on good knowledge of the subsurface velocity distribution, and thus the procedures complement each other nicely. Before showing examples of travel-time tomography, the component procedures of Iterative Tomographic Migration will be described in some detail.

1.1 TRAVEL-TIME PICKING

Travel times are, of course, the data for traveltime tomography and unless they are measured in the field they must be extracted, or picked, from the recorded seismograms. This involves digitizing across horizons on the time sections; these horizons are the trace-to-trace coherent patterns associated with reflections from the subsurface boundaries (Fig. 10). Common source records were used in this study, but there may be advantages to picking from common offset or common midpoint sorted records, or event slant-stacked records. The digitization can be done by hand with a digitizing tablet or, more automatically, on a seismic work station. Travel-time picking is an important application for seismic work stations, on which the semi-automatic picking procedures will find routine use.

1.2 RAY TRACING

Tomography is based on the approximation that the seismic energy travelling from source to receiver propagates along rays. This allows the wave equation, the partial differential equation describing energy propagation in the medium, to be reduced to ordinary differential equations for the ray path and amplitude (the eikonal and transport equations; Aki & Richards 1980, p. 84 ff.). Modelling the energy propagation through the medium by ray tracing amounts to solving the ray equations for a given background velocity model, a set of reflecting boundaries, and a collection of source/receiver pairs. The rays are assumed to reflect only from the specified reflecting boundaries, but not from velocity jumps resulting from discretization of the media bounded by the reflectors.

The ray-tracing code used in the synthetic reflection tomography example is based upon

an algorithm in which the solution to the two-point boundary value problem for the ray equations is found by 'shooting' upwards from the reflecting surface. This helps to mitigate some of the ill-posedness associated with boundary value solvers which are based upon initial value methods. Together with various techniques for adaptively smoothing internal boundaries and interpolating travel times, this ray tracer is found to be extremely robust as well as computationally efficient.

1.3 TOMOGRAPHIC INVERSION

Once travel times have been picked and rays have been traced through a model, one must solve a large system of travel-time equations for the unknown slowness perturbation vector (equation 2). The elements of the matrix D_{ij} correspond to the distance the ith ray travels in the jth cell. Since a given ray intersects only a very small portion of the model, most of the elements in that row are zero. Thus the matrix D is very sparse. In fact, the more cells a model has, the more sparse D tends to be. The reflection tomography example to be shown is roughly 99 per cent sparse. By taking advantage of this sparsity one can achieve huge improvements in run-time and memory requirements.

For relatively small problems the Singular Value Decomposition (SVD) of Golub & Reinsch (1971) is very effective. But since SVD produces large, dense matrices (the singular vectors and the intermediate matrices in the bidiagonalization procedure) it is unsuitable for large problems. Further, due to the combination of noisy data and considerable ill-conditioning, traditional least-squares methods may yield unphysical solutions, i.e. solutions which fit the data reasonably well but exhibit large, high frequency oscillations. In order to deal with these problems a sparse l_p solver was developed (Scales, Gersztenkorn & Treitel 1987; Scales 1987). This algorithm is based upon a form of preconditioned conjugate gradient in which the preconditioner is determined adaptively by the data. Minimization in the $p = 1$ norm was found to be superior to ordinary least-squares inversion whenever noise and ill-conditioning were significant. The technique is called IRLS for iteratively reweighted least-squares.

1.4 MIGRATION

Kirchhoff migration has been chosen since it is both fast and accurate. The results are virtually indistinguishable from full, finite-difference, reverse-time depth-migration. In addition, Kirchhoff migration is sufficiently fast (in 2-D) that the migration can be done interactively on real data cases of typical size. The particular implementation of Kirchhoff migration used here is due to Gray (1986).

The idea of migration is to propagate the observed seismic wavefield (or a CDP-stacked version thereof) backwards in time to the point at which a reflection occurred; in this way an image of the subsurface reflectivity (essentially jump discontinuities in the velocity) can be produced. Kirchhoff migration was developed by French (1975) and Schneider (1978). A modern, theoretical treatment can be found in Beylkin (1985), who discusses the connection between migration and inverse scattering.

For reasons of computational efficiency we use the post-stack version of Kirchhoff migration. For a discussion of the limitations of CDP processing see Schneider (1984). The extension of Kirchhoff migration to the before-stack case is, in principle, straightforward -- provided one has a big enough computer. The pre-stack problem is described, for example, in Clayton & Stolt (1981); Cohen, Hagen & Bleistein (1986); and Beylkin (1985).

2 Computational examples

We will now show numerical examples of both standard transmission tomography and Iterative Tomographic Migration. The first example is a synthetic borehole to borehole experiment. The second example is a synthetic reflection survey with a complicated salt-dome feature. The final example is a real reflection survey from an overthrust belt area.

2.1 TRANSMISSION TOMOGRAPHY

As indicated previously, transmission tomography includes surface-to-borehole as well as borehole-to-borehole geometries, as illustrated in Fig. 3. Surface-to-borehole tomography is a special case of Vertical Seismic Profiling (VSP). Whitmore & Lines (1986) show that tomography can be used to estimate seismic velocities near a wellbore by using VSP direct arrivals. We now present an example of synthetic borehole-to-borehole tomography.

The velocity blocks for this model are grey-scale coded and plotted in Plate 1, and the source receiver geometry which was used to create the travel-time data set is illustrated in Fig. 4. With this recording geometry, two different experiments tested straight-ray tomography.

In the first experiment, straight rays were traced through the true model; the resulting

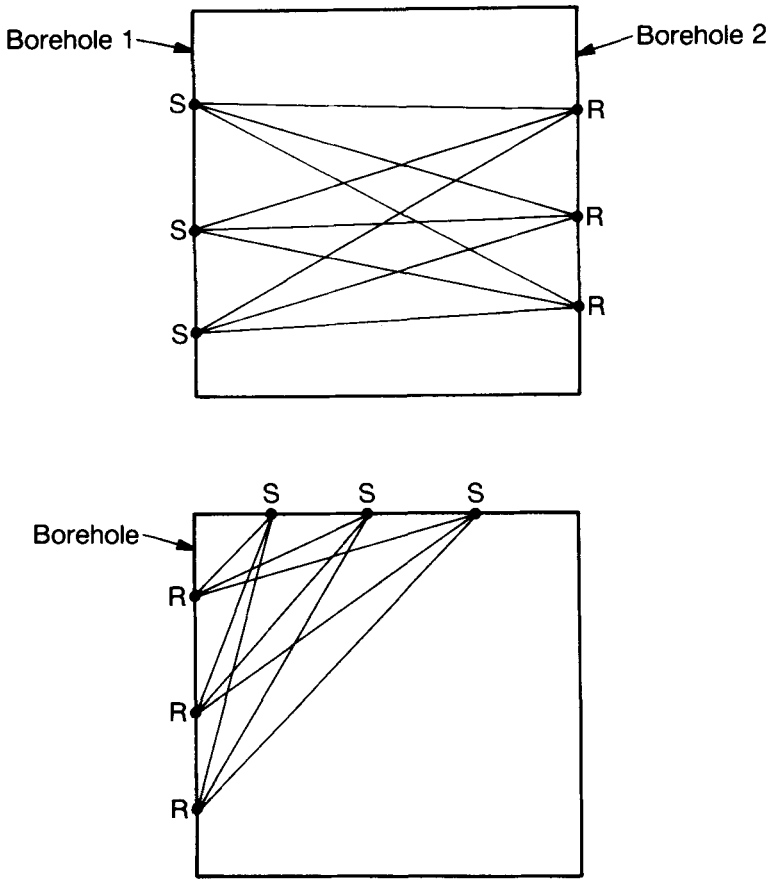

Figure 3. Typical borehole-to-borehole and surface-to-borehole geometries. (After McMechan 1983.)

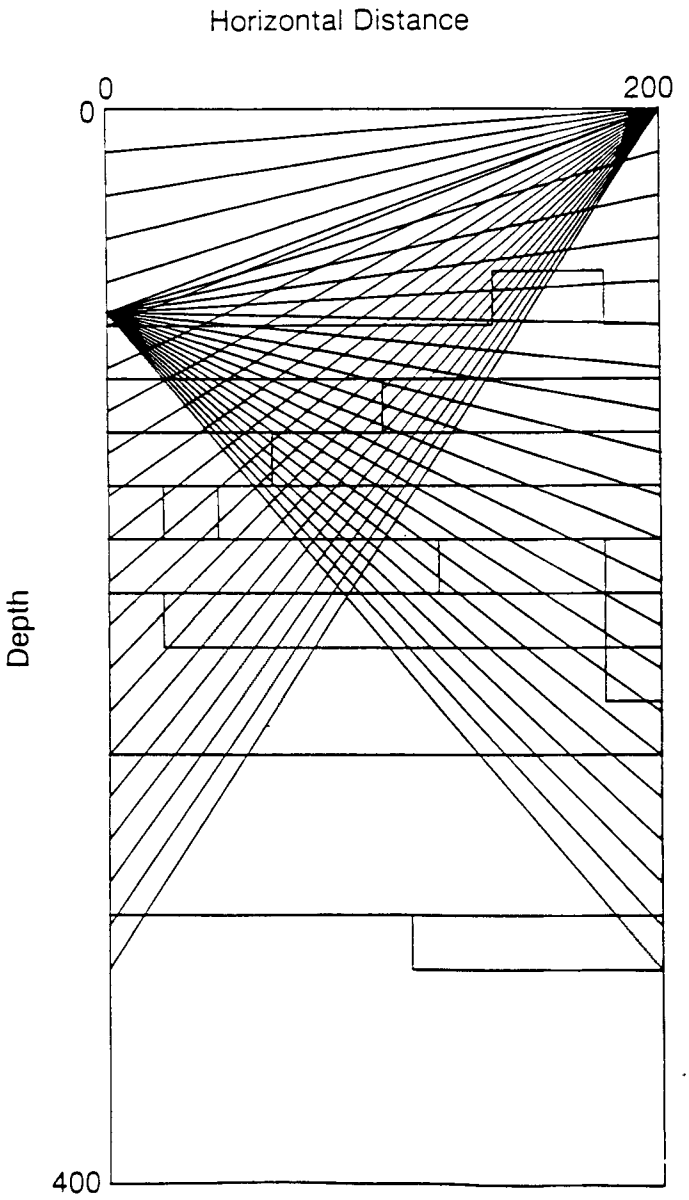

Figure 4. 42 of the 400 straight rays illuminating the model shown in Plate 1.

travel times were taken to be the observed data. The model included 420 rays and 200 cells (20 rows and 10 columns). The initial model consisted of a constant velocity of 20 (arbitrary units) in the unknown region between rows 3 and 17. On the other hand velocities were frozen at their correct values along the borehole (columns 1 and 10). Straight ray paths were then traced through the first-guess model, and Eq. (2) was solved by use of the Singular Value Decomposition (SVD) algorithm. This approach tested the imaging properties of straight rays, given straight ray data. The results shown in Plate 2 indicate that the reconstruction was excellent.

The second experiment simulated a more realistic observed data set. It was constructed by computing finite-difference acoustic wave equation synthetic traces (Kelly *et al.* 1976) for the same subsurface model and recording geometry used in the first example. First-arrival travel-times were then picked from the synthetic traces. These travel-times were taken to be the observed data. Straight rays and the SVD algorithm were again used to reconstruct the cell velocities. As one might expect, the straight ray tomogram of Plate 3 does not perfectly reconstruct the subsurface model. There are two reasons for this: first, straight rays do not satisfy Snell's law, and secondly, the travel-times were picked from synthetic traces, so that picking errors occur. Nevertheless, the velocity reconstruction of Plate 3 is more accurate than a simple interpolation of the known velocities between the two boreholes. This encouraging result, as well as much published literature, indicates that tomography can be used to estimate seismic velocities between boreholes. Similar conclusions were reached by Bois *et al.* (1972), Dines & Lytle (1979), Mason (1981), Ivansson (1982), and Peterson, Paulsson & McEvilly (1985), among others.

2.2 REFLECTION TOMOGRAPHY – FINITE DIFFERENCE EXAMPLE

The concept of reflection tomography is shown in Fig. 5. The subsurface model is covered with cells of constant slowness. Curved rays are traced from the source to the reflecting interface and back to the receiver. The reflecting interfaces are assumed to be known at each step of the procedure; they are fixed by choice (or a preliminary depth migration) for the initial step, and by depth migration at subsequent steps. Our procedure uses tomography only to image the velocity field. An alternative is to employ least-squares techniques to image the velocities and the reflector positions simultaneously, which is the approach of Bishop *et al.* (1985).

As has been remarked earlier, the iterative use of tomographic velocity determination

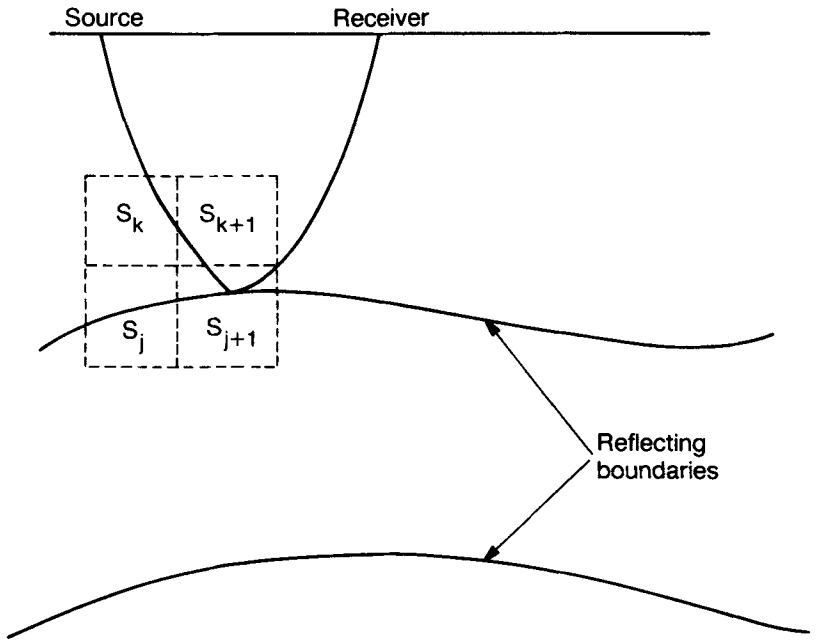

Figure 5. Schematic illustration of reflection tomography geometry. (After Bishop *et al.* 1985.)

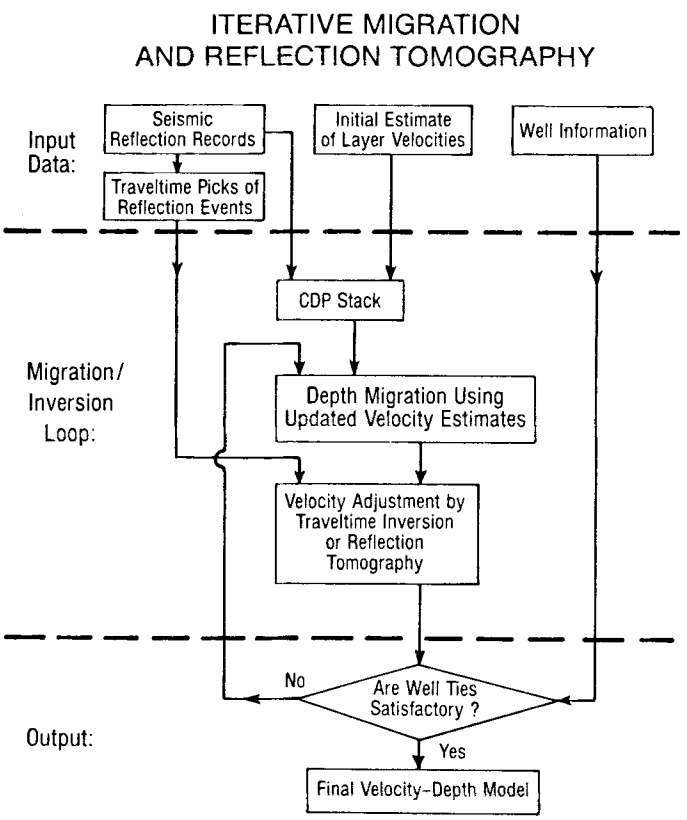

Figure 6. Flow diagram for Iterative Tomographic Migration. Velocities are determined by reflection tomography; boundaries are determined by reverse-time depth migration.

followed by depth migration is called 'Iterative Tomographic Migration'. Its processing flow is shown in Fig. 6. The method combines the ability of tomography to extract the heterogeneous subsurface velocity field with the ability of depth migration to image the subsurface interfaces. Further, depth migration is a numerically robust procedure which uses all of the seismic data, not merely the travel times, and its performance tends to improve as the subsurface velocity estimates undergo refinement by tomography.

The first step of our procedure involves picking travel-times from the unstacked data. Our travel-times were picked from common source gathers, but in some cases it may be more appropriate to make picks from common offset or common depth point-sorted data. Since stacking velocity and interval velocity are functionally related, one may wish to recompute the CDP stack for each tomographically updated interval-velocity solution. After each CDP stack, the data are depth migrated; this step produces the updated positions of the subsurface reflecting boundaries. Finally, the updated reflector positions and the updated velocity tomogram are used as input for the next tomographic velocity estimation. The iterative procedure continues until the migrated section agrees approximately with the velocity depth model. Of course, perfect agreement cannot generally be expected! Alternatively, if well information exists, the procedure is repeated until the model agrees with the available well ties. Our experience has been that the number of tomography–migration steps required to get reasonable convergence is very small, perhaps only one or two.

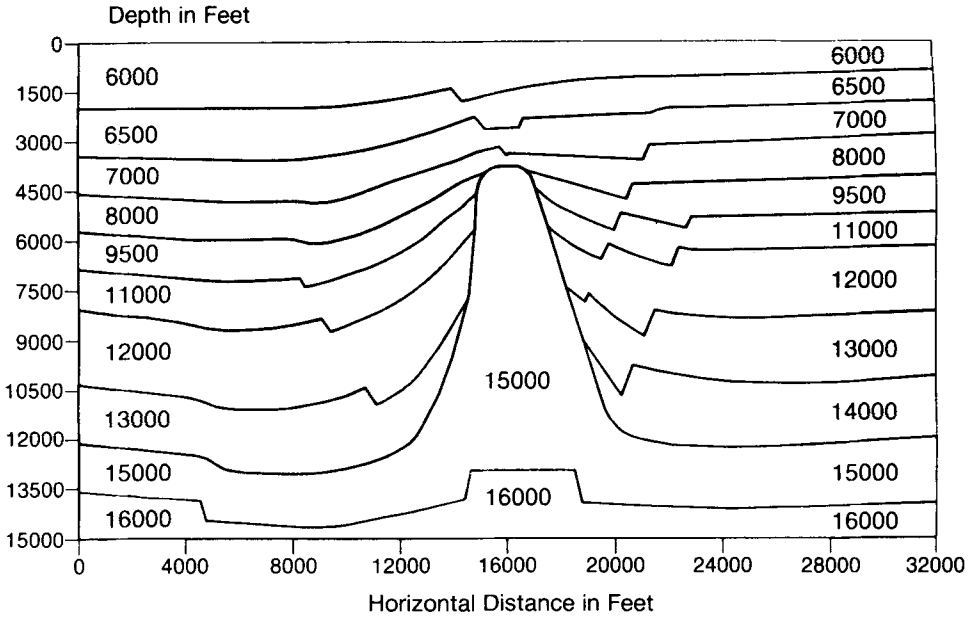

Figure 7. Geological model used for reflection tomography example. The velocities are shown between layers.

Iterative Tomographic Migration will now be illustrated with a set of synthetic common source gathers computed for the model of Fig. 7. Our choice for the depth migration algorithm was the Born–Kirchhoff technique (Gray 1986). This algorithm produces results which are virtually indistinguishable from reverse-time finite difference migration, yet it is fast enough to run interactively.

2.2.1 Initial migration and travel-time picking

The initial velocity model used consists of flat, constant velocity layers, whose velocities were chosen to be correct on the *left* side of the model. A CDP stack for this velocity model is shown in Fig. 8; the resulting depth migration is shown in Fig. 9. As expected, this migration for a flat layer velocity function provided a good reconstruction on the left-hand side of the dome, but did not accurately image the salt dome nor the deeper layers on the *right* side of the model. Run time for this migration (414 traces, 512 samples per trace) was just over one minute of cpu on the IBM 3090 scalar computer.

Our objective was to produce an accurate velocity tomogram and to improve these flat layer migration results by migrating the data with the tomographically determined velocities. The first step involved choosing a set of equally spaced common source records, and then picking a set of travel times for the reflectors. In this procedure, there were 10 events (maximum) on 9 records of 122 traces; of these, a subset of 4468 travel times was reliably picked. The traveltime picks were obtained by using digitizing tablets and a work station. Fig. 10 shows some of the common source records from which event times were picked. The next step involved tracing rays through the flat layer model, from which we computed the resulting travel times and ray-cell distances D_{ij}.

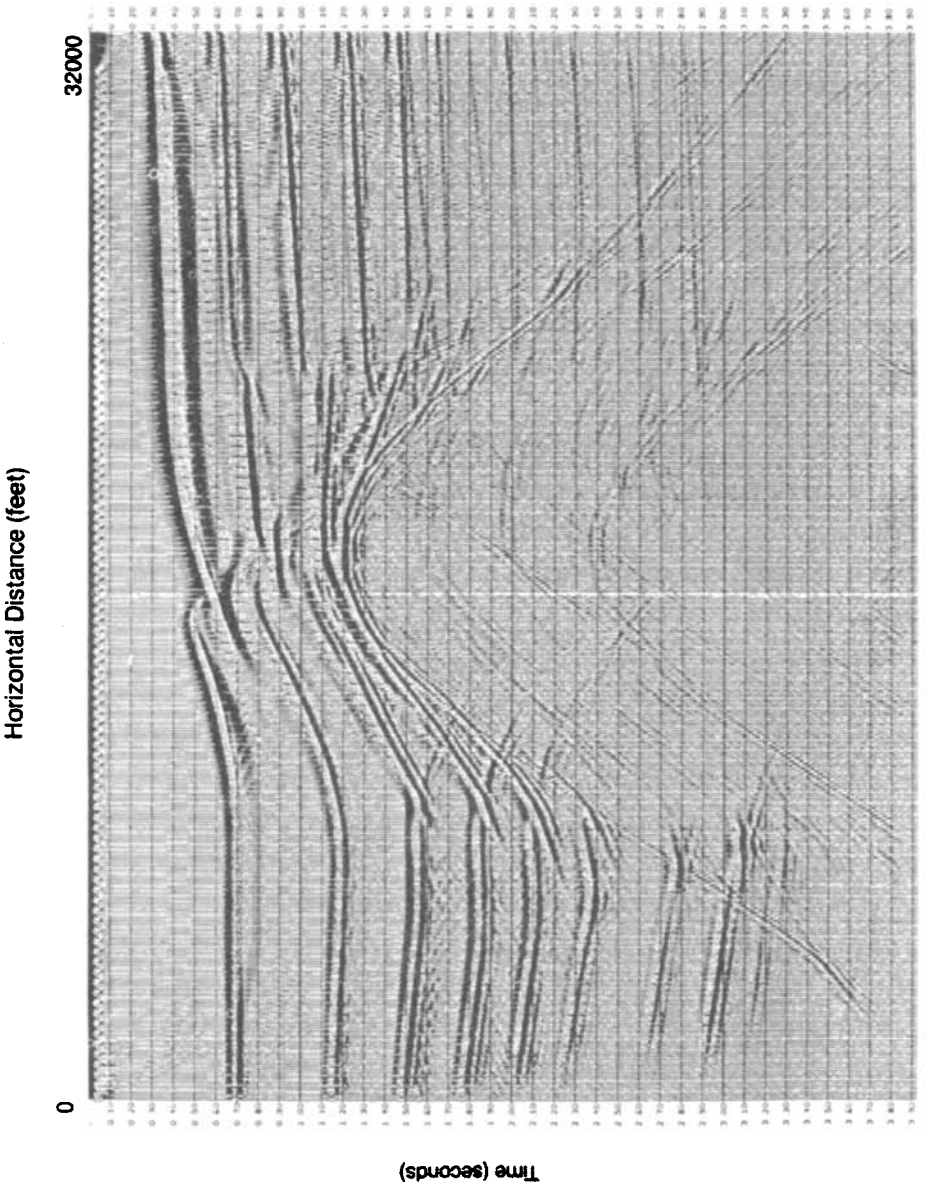

Figure 8. CDP stack using flat-layer velocity model.

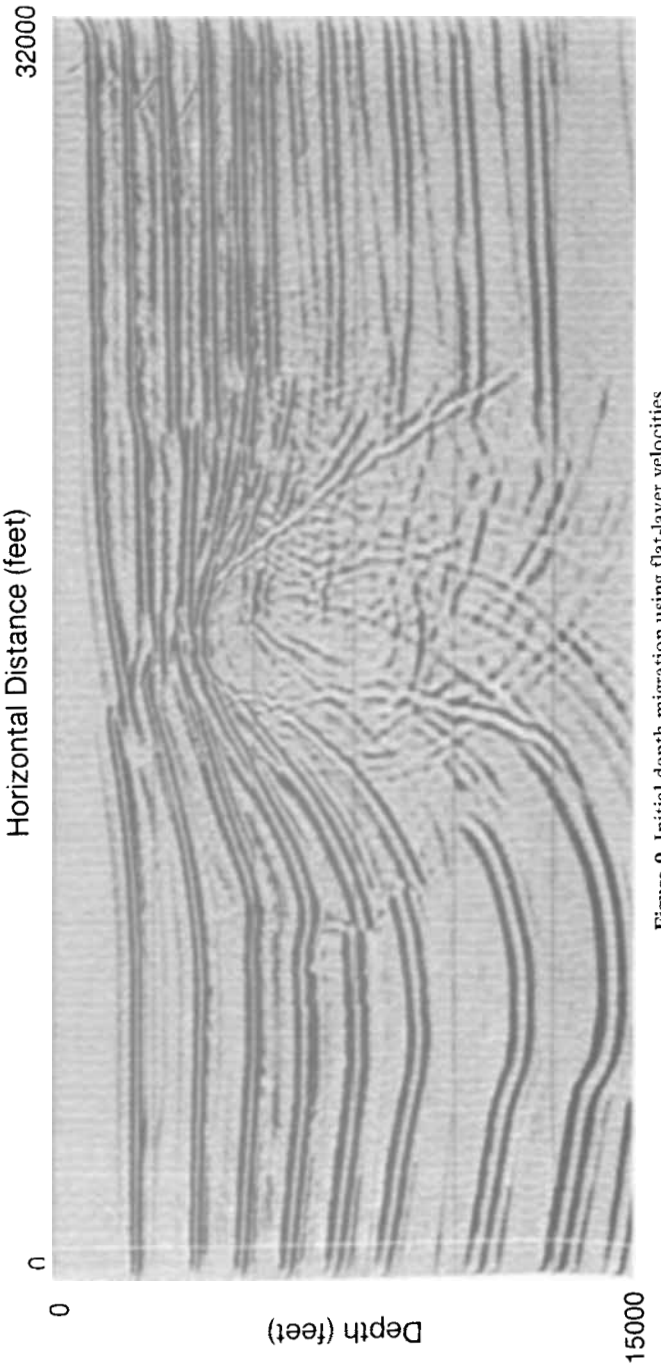

Figure 9 Initial depth migration using flat-layer velocities.

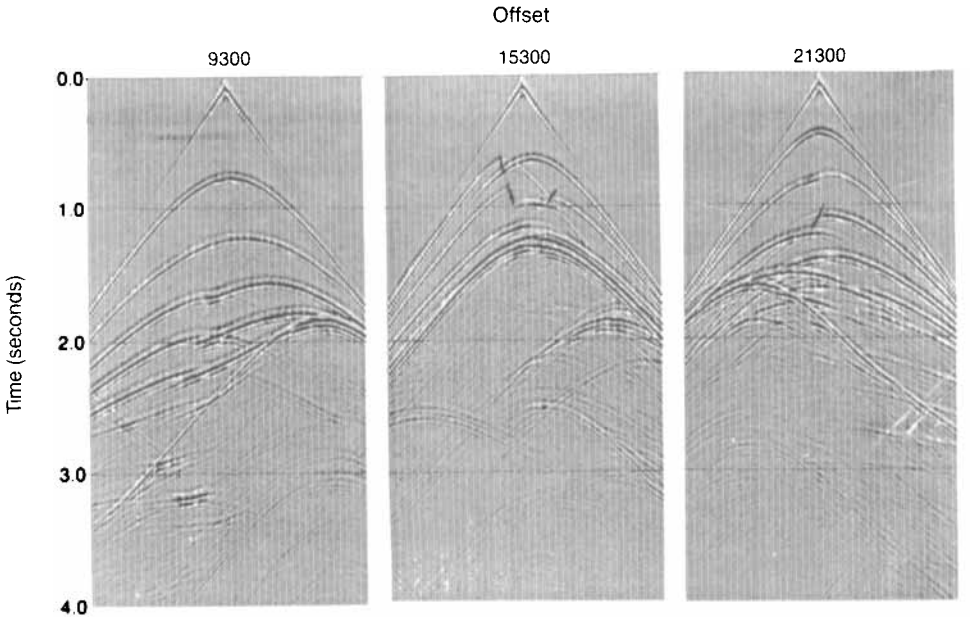

Figure 10. Finite difference common source gathers at offsets of 9300, 15300, and 21300. Travel-time picks were made on peaks just below horizons.

2.2.2 Ray tracing for the model

The model was covered with 3200 (40 × 80) cells of size 400 by 400 ft. Fig. 11 shows examples of the rays traced for three reflectors. The computation time was about 0.01 s ray^{-1} on an IBM 3090 scalar computer.

2.2.3 Tomographic inversion

Following the estimation of reflected travel times (from the 'data') and the computation of travel times for the initial model, (2) was solved for the slowness perturbations Δs. Only cells which are adequately illuminated contribute significantly to the inversion. The dimensionless illumination of the jth cell is defined to be the sum of the elements in the jth column of D divided by the cell size. This gives an approximate number of rays per cell. (Note that rays which graze cells do not contribute significantly to its illumination.) A somewhat better heuristic measure of resolution, currently being implemented, is to combine the ray illumination with the angular spread of that illumination. Thus a cell in which all of the rays are nearly parallel is given a relatively small weight. The number of rows in the D matrix equals the number of reliable travel-time picks (4468), and the number of columns equals the number of cells used to cover the model (3200). The D matrix is large (4468 × 3200) and sparse (about 1 per cent of the elements are non-zero). For a problem of this size, the use of SVD is generally out of the question, therefore sparse iterative solvers are employed. Fast iterative methods such as the l_p version of the preconditioned Conjugate Gradient (Scales *et al.* 1987) proved to be most effective on this problem. Solution times were about 5–10 cpu s on the IBM 3090 scalar computer. The slowness perturbations were then added to the original slowness model to give the updated slowness solution. As a final step a fine-grain median filter is usually applied to the output velocity model in order to

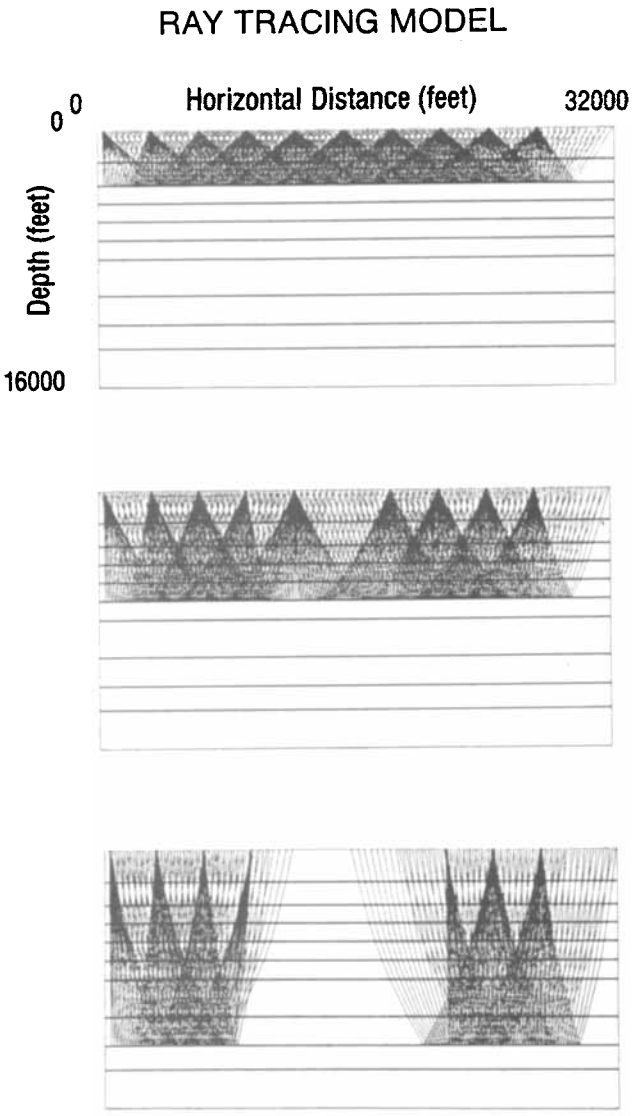

Figure 11. Sample curved-ray illumination of flat layer initial approximation.

smooth the solution for the next stage of the iterative inversion. Median filters (Gersztenkorn & Scales 1987) are extremely useful smoothers for computed tomograms. They ignore outliers instead of averaging them into the solution. Further, median filters preserve edges, ubiquitous features in the models of exploration seismology.

The initial flat-layer model is shown in Plate 4a. The exact solution and the tomographic reconstruction are shown in Plate 4b and Plate 5a. Plate 5b shows the amount of illumination present. In other words, cells can only be illuminated by rays for which there are reliable travel-time picks. If there are no picks for a certain portion of the model, it is impossible to image that region tomographically.

The tomographic solution is a much better representation of the velocity depth model than the original flat layer guess. Nevertheless, it has two important limitations, namely the

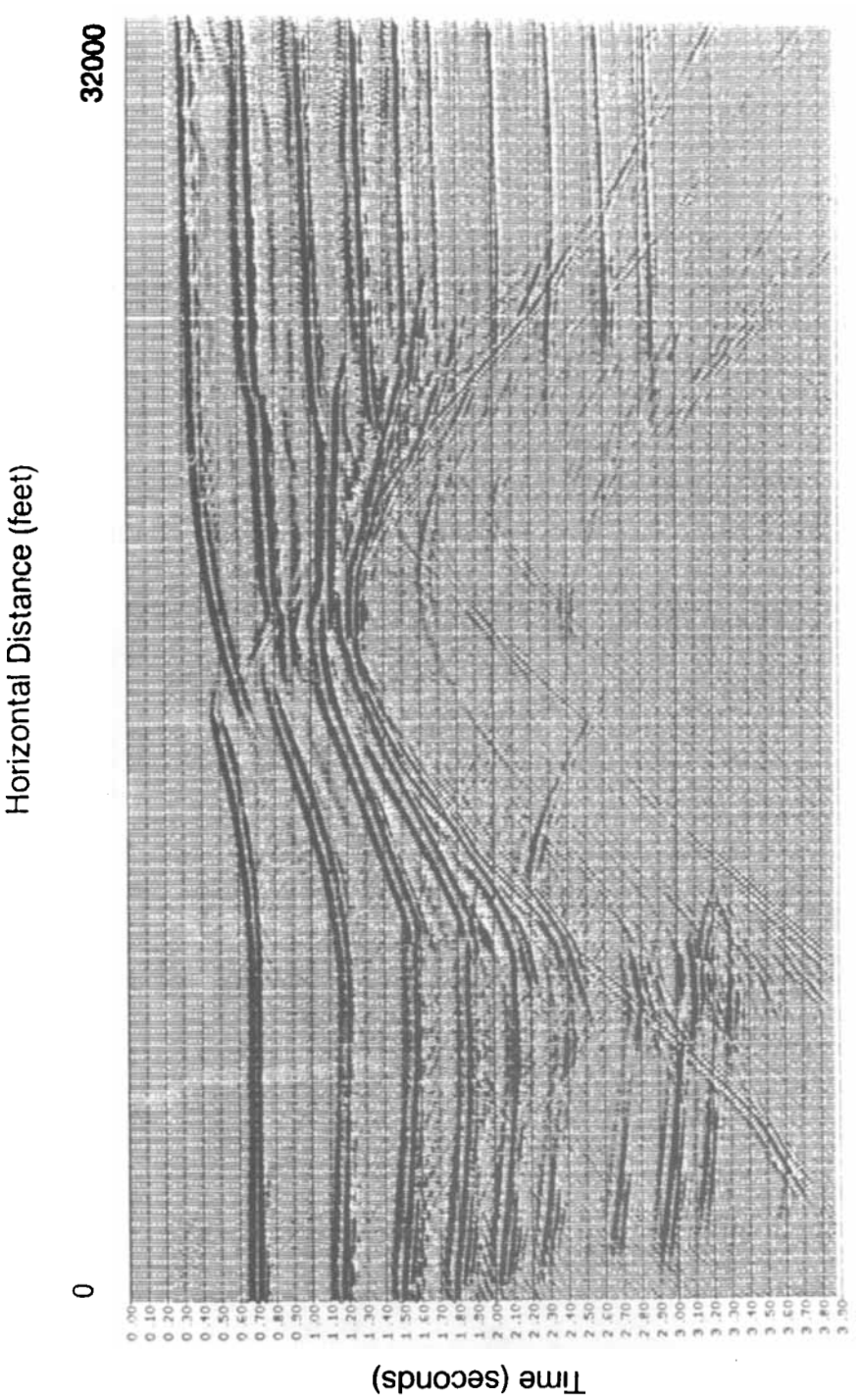

Figure 12. CDP stack using tomographically determined velocities.

extent to which travel times can be picked, and the limited aperture of illumination available.

2.2.4 Final migration

The CDP stack was recomputed by using the new, tomographically determined, velocity-depth model. This new CDP stack is shown in Fig. 12 and shows a definite improvement over the CDP stack computed from the initial flat layer velocity model, Fig. 8. The new CDP stacked section was then depth migrated with the tomographically determined velocities. The resulting depth migration (overlain by the tomogram in Plate 6) shows a much improved image of the salt dome flanks compared to Fig. 9. The only portion of the model not successfully imaged was the horst block below the dome. This feature cannot be resolved by standard CDP processing since ray tracing indicates that reflected rays for common midpoint source–receiver pairs do not reflect off the horst at a common depth

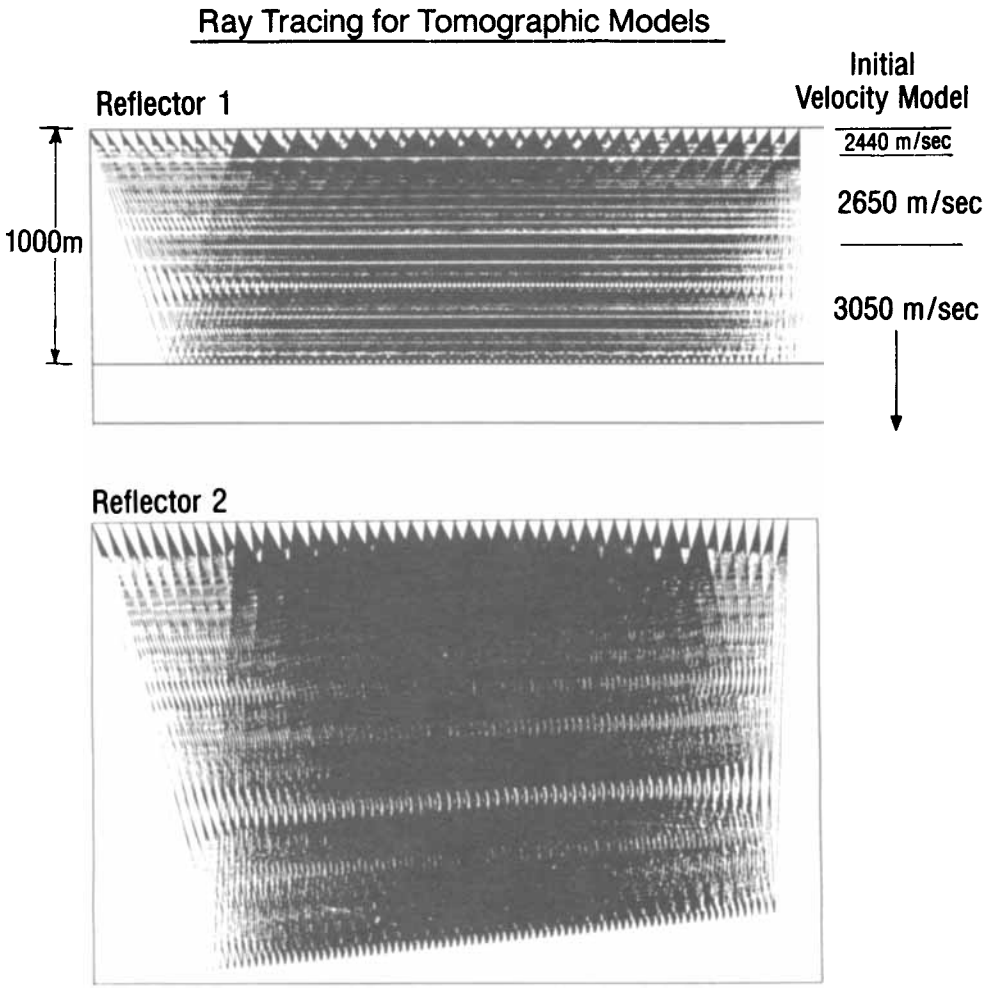

Figure 13. Velocity model and straight ray illumination used for real data example. A three-layer velocity model was used, velocities are shown on the right. Travel times were picked for the two reflectors shown.

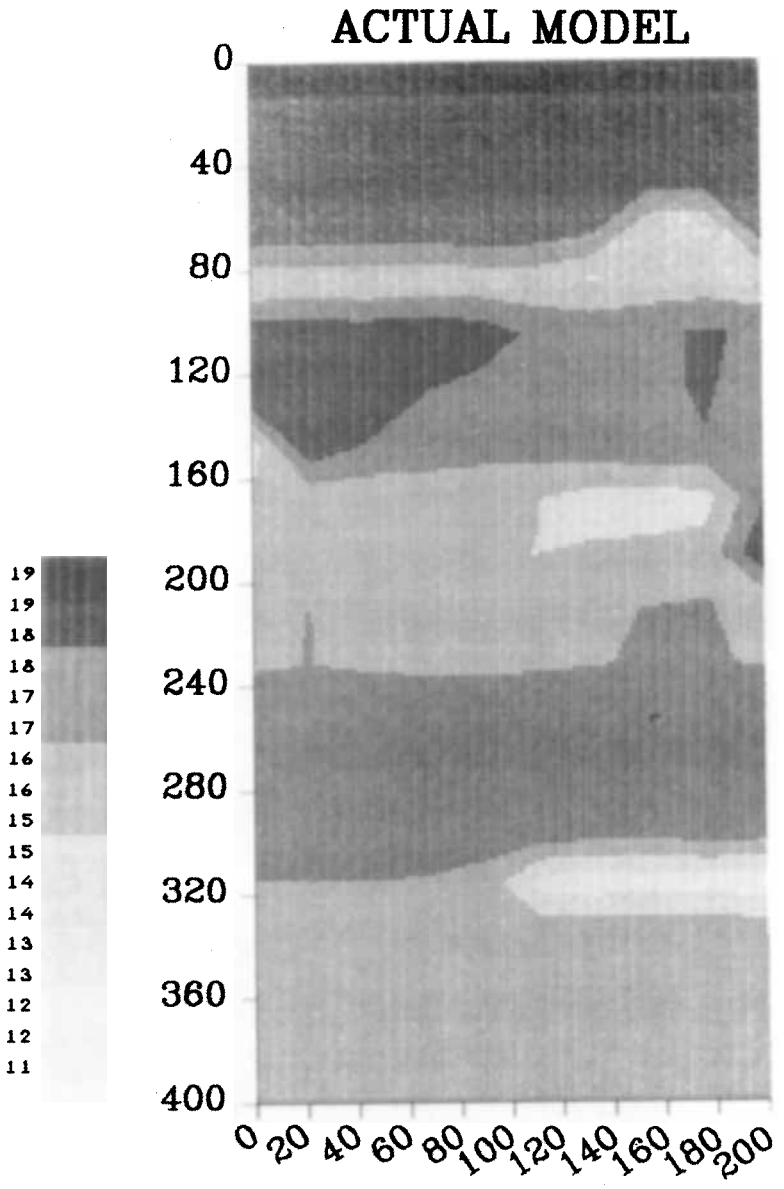

Plate 1. Grey-scale coded velocity model for transmission tomography example. Synthetic data were produced by finite-difference wave equation modelling through this model. Velocity scale at left.

[*facing page* 300]

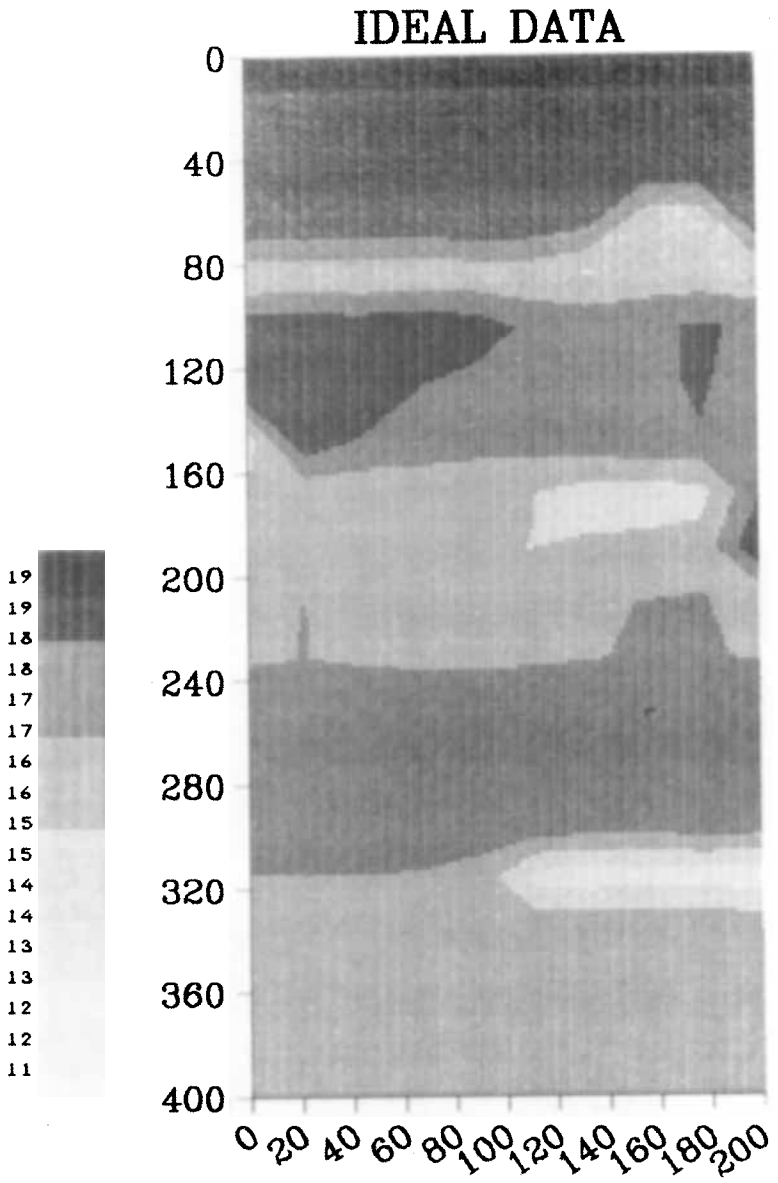

Plate 2. SVD inversion with straight ray data and straight ray modelling.

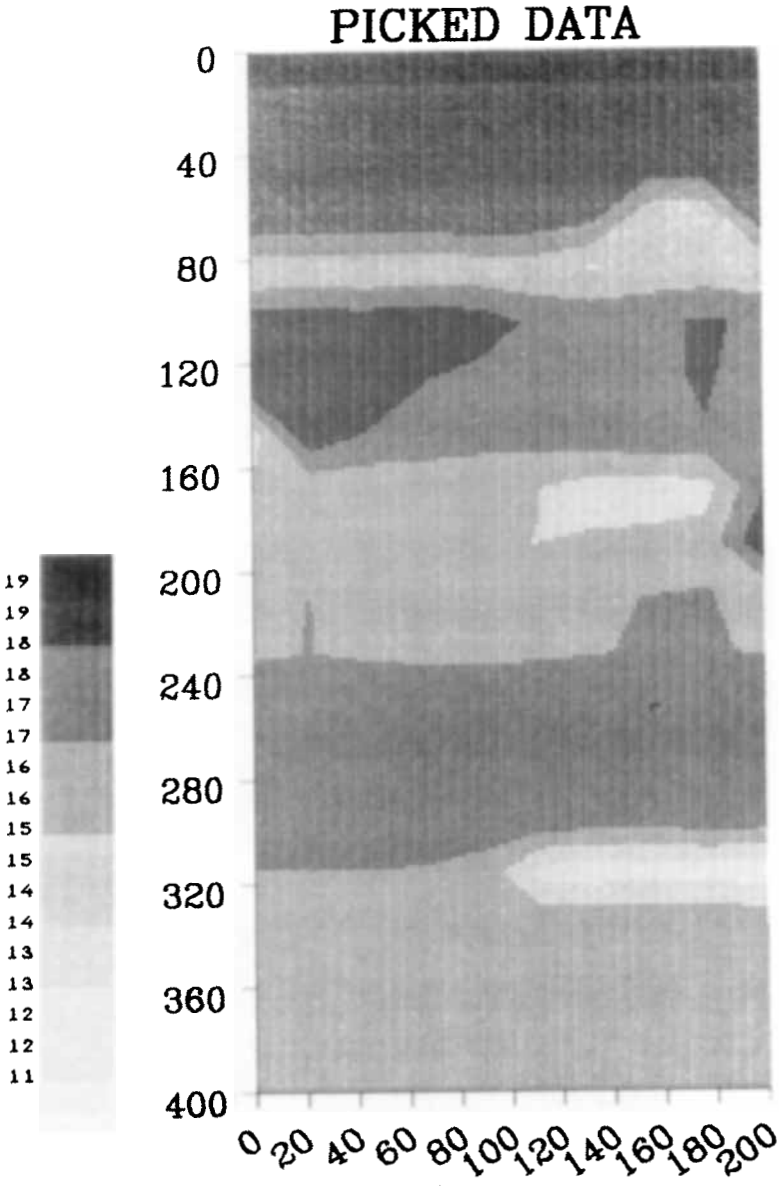

Plate 3. SVD inversion with finite difference data and straight ray modelling.

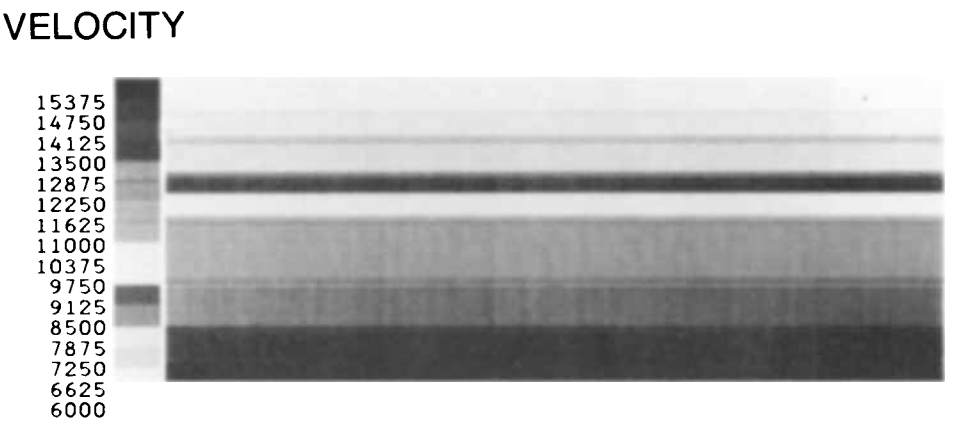

Plate 4a. Grey-scale coded flat-layer initial velocity model used in reflection tomography example. Velocity scale is on the left.

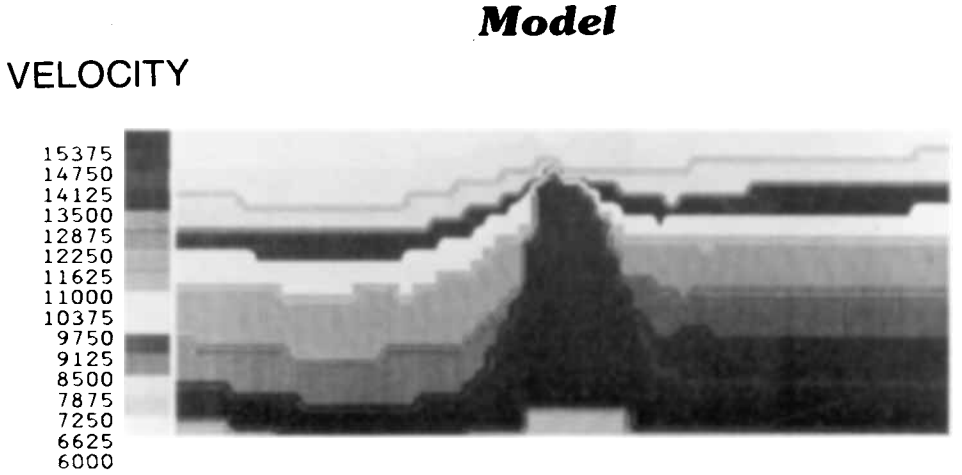

Plate 4b. Velocity model used in synthetic reflection example.

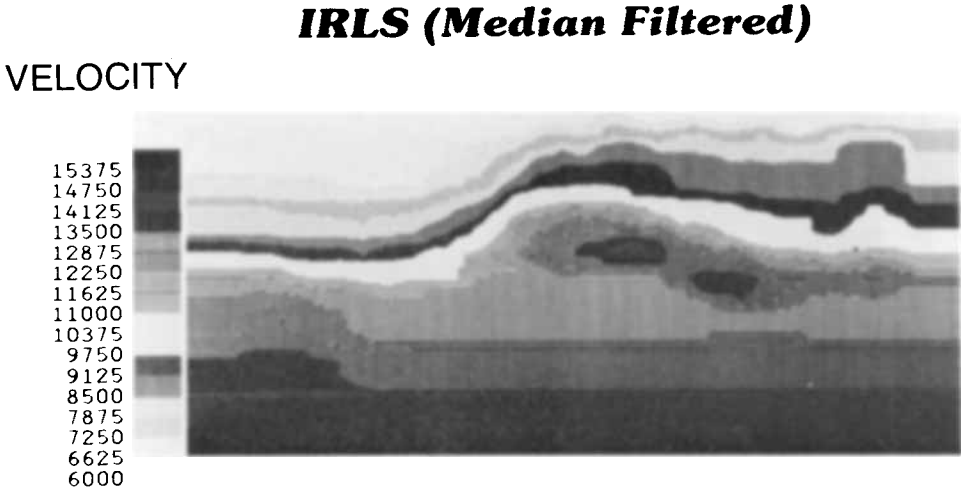

Plate 5a. Median filtered computed tomogram.

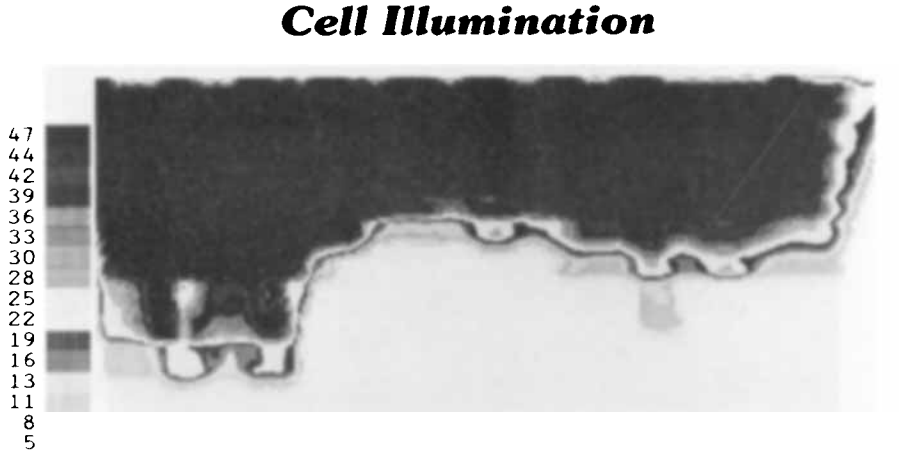

Plate 5b. Dimensionless cell illumination. Unilluminated regions are due to lack of reliably picked traveltimes.

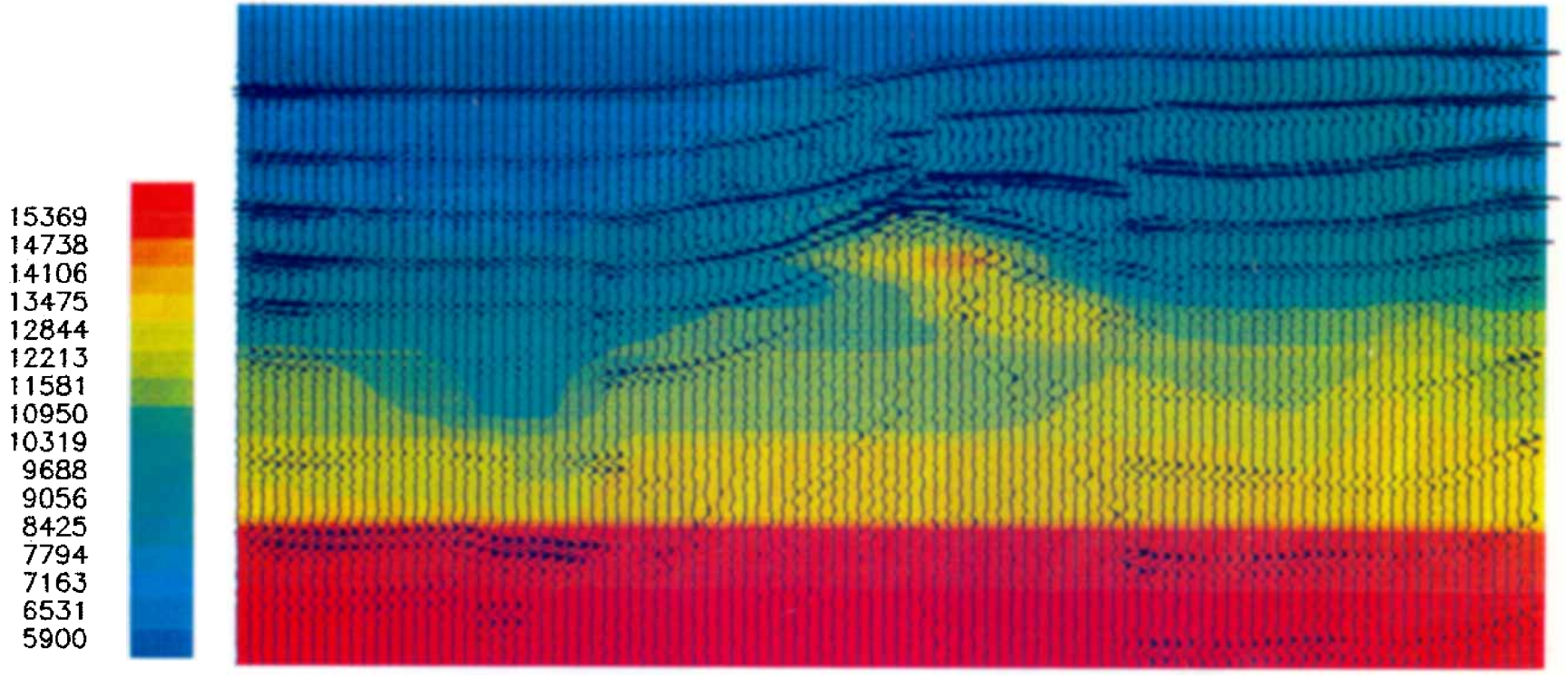

Plate 6. Depth migration using tomographically determined velocities overlain by the computed tomogram. Computed velocities are shown in colour, ranging from 6000 f s^{-1} (blue) to 1600 f s^{-1} (red). Geologic layers are shown in black.

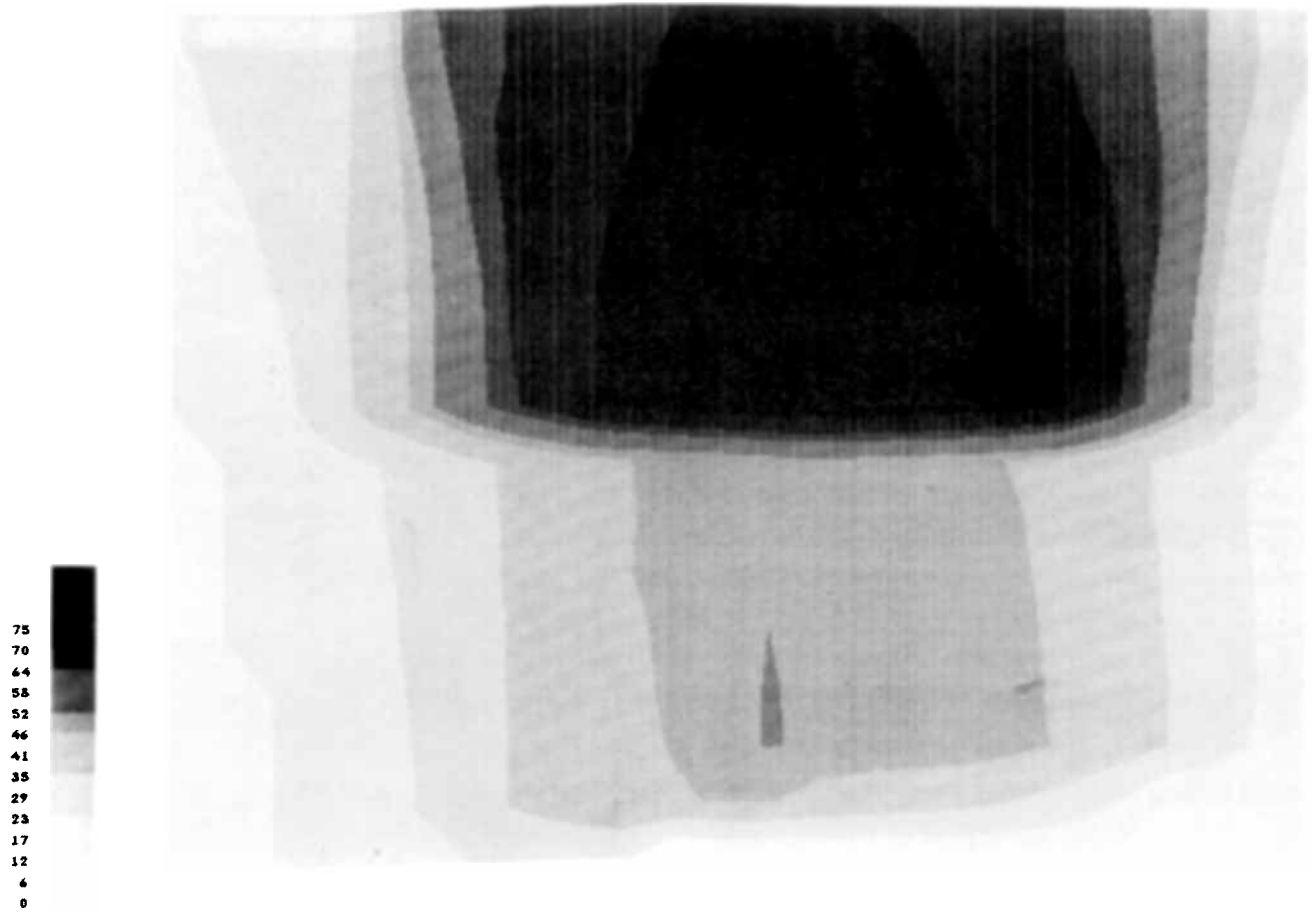

Plate 7. Dimensionless cell illuminations for real data case. Unilluminated regions due to lack of reliably picked travel times.

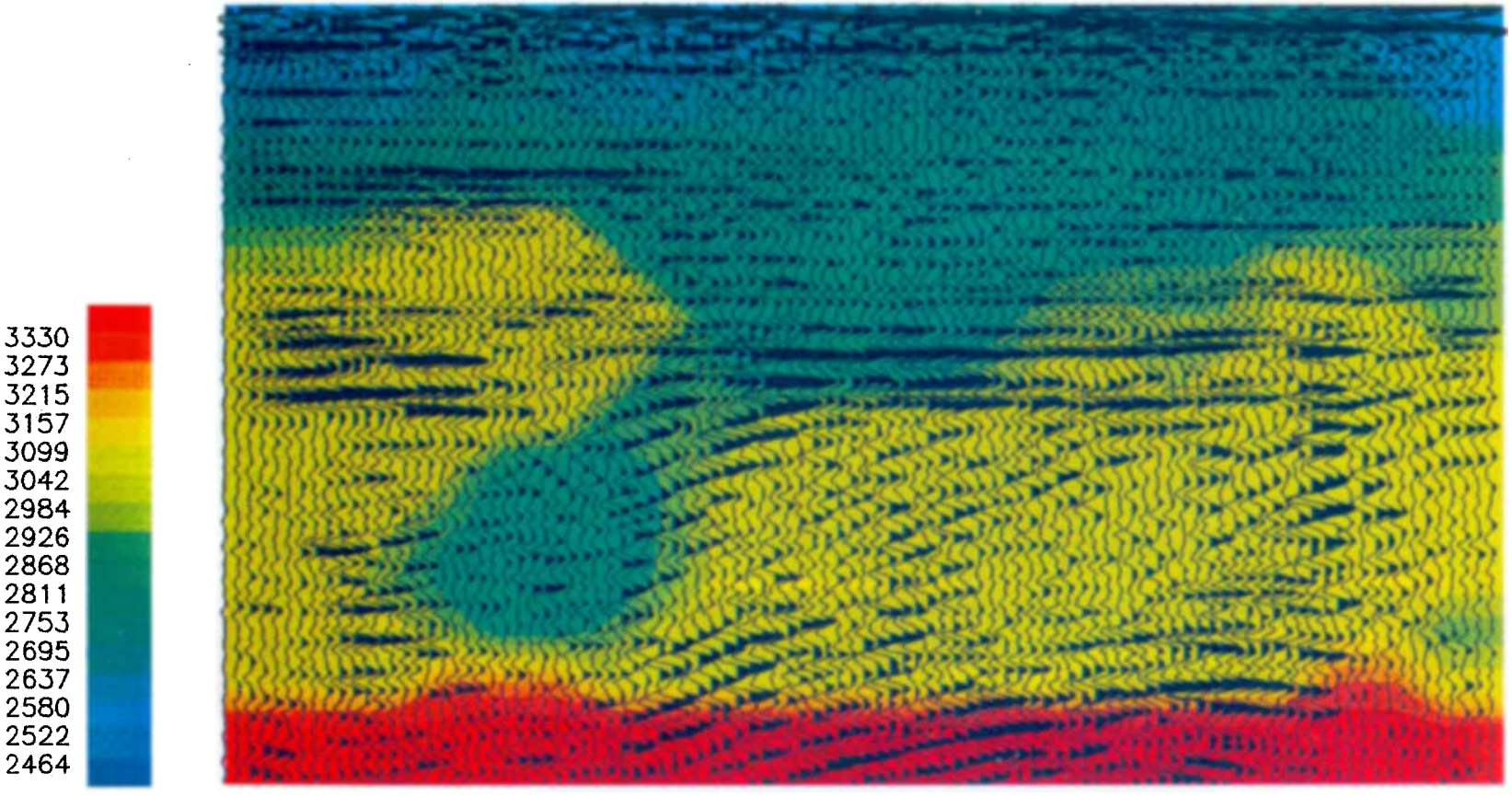

Plate 8. Velocity tomogram superposed on the migrated depth section. Computed velocities are shown in colour, ranging from 2400 m s^{-1} (blue) to 3400 m s^{-1} (red).

point. In this case, a single step of Iterative Tomographic Migration produced good agreement with the known velocity–depth model.

2.3 REFLECTION TOMOGRAPHY – REAL DATA EXAMPLE

Following the successful experiments on synthetic data, we now conclude with an example of Iterative Tomographic Migration applied to real data. This data case was recorded in an overthrust belt area, therefore accurate velocities are needed to image the dipping and folded geologic layers. In the initial step of the tomographic process, 1475 travel times were picked from common source data using a seismic work station. The basic tomographic model consisted of 384 velocity cells (16 rows and 24 columns) and two reflectors. The cells were chosen to be 122 m-sided squares. Fig. 13 displays the ray tracing models for the two reflectors as well as the initial velocity model for the tomographic inversion. Plate 7 indicates the relative ray illumination for the model.

The computed velocity model was used in producing the stacked section and subsequent depth migration shown in Fig. 14. The computed velocity model and the depth migration are superposed in Plate 8. The velocity tomogram is shown with colour-coded velocities and the geologic layers are shown in black. The region shown is about 3100 m across and 1900 m deep. The subsurface image produced by tomography and depth migration agrees with the conventional processing and modelling carried out previously. The depth migration shows a

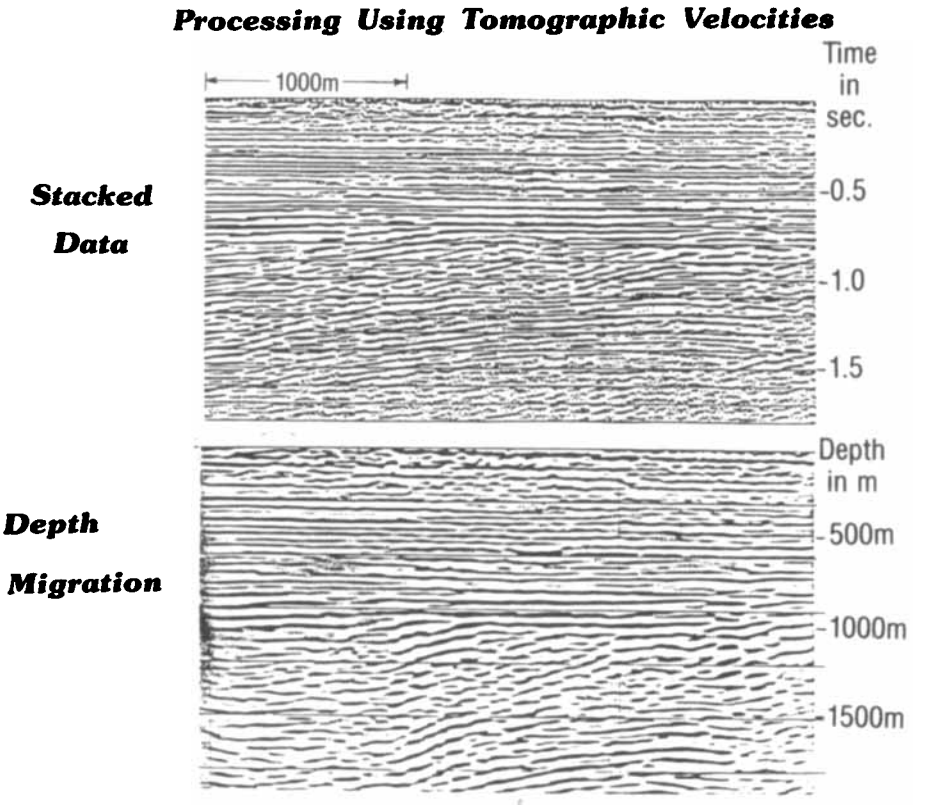

Figure 14. CDP stack and depth migration for real data case, both computed with the tomographically determined velocities.

series of dipping layers which underlie a set of flat shallow layers. In the bottom right hand corner of the section, there is evidence of a recumbent fold, which is also evident from conventional processing and modelling. This result indicates that Iterative Tomographic Migration is an effective technique for inverting complex reflection data.

3 Conclusions

We have shown that traveltime tomography provides reliable seismic velocity estimates for both reflected and transmitted arrivals. Travel-time tomography can be used as a stand-alone imaging technique (as in borehole-to-borehole tomography), as a means of providing good-input velocity models for depth migration, or iteratively with depth migration in the manner which we have called Iterative Tomographic Migration. In these various forms, tomographic techniques can be used to efficiently image complex structures.

Acknowledgments

We would like to thank Sam Gray for providing his migration code and helping to adapt it to our needs. We would like to thank Ron Nelson and Red Sheffield for proposing the transmission model. For the reflection example we would like to thank Carl Regone for proposing the model and Lajuanta Young and Dan Whitmore for doing the finite difference modelling. Thanks also go to Mike Sabroff, Rhoda Bucker, and Coreen Marson for their help with colour graphics and seismic processing. Finally we would like to thank Dan Whitmore and John Gallagher for useful discussions.

References

Aki, K. & Richards, P., 1980. *Quantitative Seismology*, Freeman, London.

Beylkin, G., 1985. Imaging of discontinuities in the inverse scattering problem by inversion of a causal generalized Radon transform, *J. Math. Phys.*, **26**, 99–108.

Bishop, T., Bube, K., Cutler, R., Langan, R., Love, P., Resnick, J., Shuey, R., Spindler, D. & Wyld, H., 1985. Tomographic determination of velocity and depth in laterally varying media, *Geophysics*, **50**, 903–923.

Bois, P., La Porte, M., Lavergne, M. & Thomas, G., 1972. Well to well seismic measurements, *Geophysics*, **3**, 471–483.

Cassell, B., 1982. A method for calculating synthetic seismograms in laterally varying media, *Geophys. J. R. astr. Soc.*, **69**, 339–354.

Christoffersson, A. & Husebye, E., 1979. On three-dimensional inversion of *P*-wave time residuals: option for geologic modelling, *J. geophys. Res.*, **84**, (B11), 6168–6176.

Clayton, R. & Stolt, R., 1981. A Born-WKBJ inversion method for acoustic reflection data, *Geophysics*, **46**, 1559–1567.

Cohen, J., Hagen, F. & Bleistein, N., 1986. Three-dimensional inversion with arbitrary reference, *Geophysics*, **51**, 1552–1558.

Deans, S., 1983. *The Radon Transform and Some of Its Applications*, Wiley, London.

Dines, K. & Lytle, R., 1979. Computerized geophysical tomography, *Proc. IEEE*, **67**, 1065–1073.

French, W., 1975. Computer migration of oblique seismic reflection profiles, *Geophysics*, **40**, 961–980.

Gersztenkorn, A. & Scales, J., 1987. Smoothing seismic tomograms with alpha-trimmed means, *Geophys. J. R. astr. Soc.*, **91**, in press.

Golub, G. & Reinsch, C., 1970. Singular value decomposition and least squares solution, *Num. Math.*, **14**, 403–420.

Gray, S., 1986. Efficient travel time calculations for Kirchhoff migration, *Geophysics*, **51**, 1685.

Gustavsson, M., Ivansson, S., Moren, P. & Pihl, J., 1986. Seismic borehole tomography – measurement system and field studies, *Proc. IEEE*, **74**, 339–346.

Herman, G., 1980. *Image Reconstruction from Projections*, Academic Press, New York.

Ivansson, S., 1984. Crosshole investigations – tomography and its application to crosshole seismic measurements, *Stripa Project*, **84-08**.

Kelly, K., Ward, R., Treitel, S. & Alford, R., 1976. Synthetic seismograms: a finite difference approach, *Geophysics*, **41**, 2–27.

Langan, R., Lerche, I. & Cutler, R., 1985. Tracing rays through heterogeneous media: an accurate and efficient procedure, *Geophysics*, **50**, 1456–1466.

Mason, I., 1981. Algebraic reconstruction of a two-dimensional inhomogeneity in the High Hazles seam of Thorseby colliery, *Geophysics*, **46**, 298–308.

McMechan, G., 1983. Seismic tomography in boreholes, *Geophys. J. R. astr. Soc.*, **74**, 601–612.

Nercessian, A., Hirn, A. & Tarantola, A., 1984. Three-dimensional seismic transmission prospecting of the Mont Dore volcano, France, *Geophys. J. R. astr. Soc.*, **76**, 307–315.

Neumann, G., 1981. Determination of lateral inhomogeneities in reflection seismics by inversion of travel-time residuals, *Geophys. Prospect.*, **29**, 161–177.

Peterson, J., Paulsson, B. & McEvilly, T., 1985. Applications of algebraic reconstruction techniques to crosshole seismic data, *Geophysics.*, **50**, 1566–1580.

Scales, J., 1987. Tomographic inversion via the conjugate gradient method, *Geophysics*, **52**, 179–185.

Scales, J., Gersztenkorn, A. & Treitel, S., 1987. Fast l_p solution of large, sparse linear systems: applications to seismic travel time tomography, *J. Comp. Physics* (in press).

Schneider, W., 1978. Integral formulation of migration in two and three dimensions, *Geophysics*, **43**, 49–76.

Schneider, W., 1984. The common depth point stack, *Proc. IEEE*, **72**, 1238–1254.

Stork, C. & Clayton, R., 1985. *Iterative tomographic and migration reconstruction of seismic images*, paper presented at the 1985 SEG meeting in Washington.

Tarantola, A. & Nercessian, A., 1984. Three-dimensional inversion without blocks, *Geophys. J. R. astr. Soc.*, **76**, 299–306.

Whitmore, N. & Lines, L., 1986. VSP depth migration of a salt dome flank, *Geophysics*, **51**, 1087–1109.

Williamson, P., 1984. *The application of tomography to the inversion of traveltime data in reflection seismology*, paper presented at the 1984 EAEG meeting in London.

Worthington, M., 1984. An introduction to geophysical tomography, *First Break*, **2**, 20–27.